

Photoinduced self-trapped hole center in TiO₂ crystals

Shan Yang (杨山), A. T. Brant, and L. E. Halliburton*

Physics Department, West Virginia University, Morgantown, West Virginia 26506, USA

(Received 21 May 2010; revised manuscript received 4 July 2010; published 21 July 2010)

Electron paramagnetic resonance is used to identify the intrinsic self-trapped hole center in bulk TiO₂ crystals having the rutile structure. Two additional extrinsic trapped hole centers associated with a defect on a neighboring Ti⁴⁺ site are also observed. For each center, the unpaired spin (i.e., the hole) is localized in a nonbonding *p* orbital on an oxygen ion. The three hole centers are photoinduced with 442 nm laser light at 4 K. After the laser light is removed, the majority of the hole centers disappear immediately at 4 K with the remainder disappearing when the temperature is raised above approximately 10 K. Angular-dependence data, taken in the three high-symmetry planes, provide spin-Hamiltonian parameters for the self-trapped hole center and one of the two defect-related trapped hole centers. The principal values of the *g* matrix for the self-trapped hole center are 2.0040, 2.0129, and 2.0277 and the corresponding principal axes are along the [110], [001], and [1 $\bar{1}$ 0] directions in the crystal. Although the principal values of the *g* matrix for the extrinsic trapped hole center are similar (2.0036, 2.0182, and 2.0307), the directions of two of its principal axes are not along high-symmetry directions in the crystal because of the neighboring perturbation.

DOI: [10.1103/PhysRevB.82.035209](https://doi.org/10.1103/PhysRevB.82.035209)

PACS number(s): 76.30.Mi, 71.38.Ht, 61.72.jn

Electron paramagnetic resonance (EPR) has been widely used to investigate trapped electrons in single crystals of titanium dioxide (TiO₂).^{1–6} Much less attention has been given to the use of EPR to identify and characterize localized holes in this technologically important material. Isolated Fe³⁺ and Cr³⁺ ions substituting for Ti⁴⁺ ions are one source of hole traps in TiO₂ crystals (these impurities trap holes and convert to Fe⁴⁺ and Cr⁴⁺ ions during exposure to short-wavelength light at low temperature).^{7–9} The majority of photoinduced holes in the TiO₂ lattice, however, are expected to be trapped at oxygen ions.^{10–12} Although the hole may be localized on an oxygen ion in the regular lattice, i.e., as a self-trapped hole, it is also possible to have the hole localized on an oxygen ion adjacent to an impurity or a cation vacancy. An example of this latter behavior is the trapped hole center in aluminum-doped GeO₂ crystals having the rutile structure. Here, EPR results¹³ show that a hole is localized in a nonbonding *p* orbital on one substitutional oxygen ion adjacent to an Al³⁺ impurity substituting for a Ge⁴⁺ ion. In follow-up studies, Zwingel^{14,15} used the EPR technique to demonstrate that the same hole-trapping behavior occurs in TiO₂ (rutile) crystals doped with either aluminum or gallium. In these doped crystals, Zwingel found that a hole is trapped at low temperature on an oxygen ion that has an Al³⁺ or Ga³⁺ impurity ion at an adjacent Ti⁴⁺ site. Recent modeling studies have focused on intrinsic hole polarons¹⁰ (i.e., self-trapped hole centers) and Al-bound hole polarons¹⁶ in both the anatase and rutile forms of TiO₂. In general, trapped holes (on oxygen ions or on acceptorlike dopant ions such as nitrogen) are expected to play important roles in the photocatalytic mechanisms occurring at the surface of TiO₂ films and nanoparticles.^{17–22}

In the present paper, EPR experiments are described that identify and characterize the intrinsic self-trapped hole center in TiO₂ (rutile) crystals. Three distinct trapped hole centers are observed when an undoped fully oxidized crystal is illuminated with 442 nm laser light while being held near 4 K. One of the three EPR spectra exhibits the symmetry of the

TiO₂ lattice and is assigned to the self-trapped hole center while the other two spectra exhibit a local symmetry lower than that of the lattice and are assigned to trapped hole centers with an adjacent defect. All three EPR signals thermally decay below or near 10 K when the laser light is removed. The principal values and the principal-axis directions of the *g* matrices for the self-trapped hole center and one of the defect-associated hole centers are obtained from complete sets of angular-dependence data. Proposed models for these centers have the hole localized in a nonbonding *p* orbital on one oxygen ion. Weak hyperfine interactions with adjacent Ti⁴⁺ ions are observed, but not analyzed, in the case of the self-trapped hole center.

A large single crystal of rutile-structured TiO₂ was purchased from CrysTec (Berlin, Germany) for use in this investigation. This undoped [001] plate had dimensions of 10 × 10 × 2 mm³ and was grown by the Verneuil technique. A set of six EPR-sized samples having approximate dimensions of 3 × 5 × 2 mm³ were cut from this larger crystal. Prior to any illumination with laser light, these samples only exhibited EPR signals from Fe³⁺ and Cr³⁺ ions at low temperature, thus indicating that they had been fully oxidized. More specifically, there were no observable EPR signals due to Ti³⁺ ions in the as-received samples. A Bruker EMX spectrometer operating near 9.45 GHz was used to take the EPR data while a helium-gas-flow system from Oxford Instruments maintained the sample temperature in the 4–30 K range. Precise values of the static magnetic field were obtained using a Bruker proton NMR gaussmeter. A small MgO crystal doped with Cr³⁺ ions was used to correct for the difference in magnetic field between the sample and the probe tip of the gaussmeter (the isotropic *g* value for Cr³⁺ in MgO is 1.9800). Narrow slots in the end of the Bruker TE₁₀₂ rectangular microwave cavity allowed optical access to the sample. Approximately 15 mW of 442 nm light from a He-Cd laser was incident on the sample during the low-temperature illuminations.

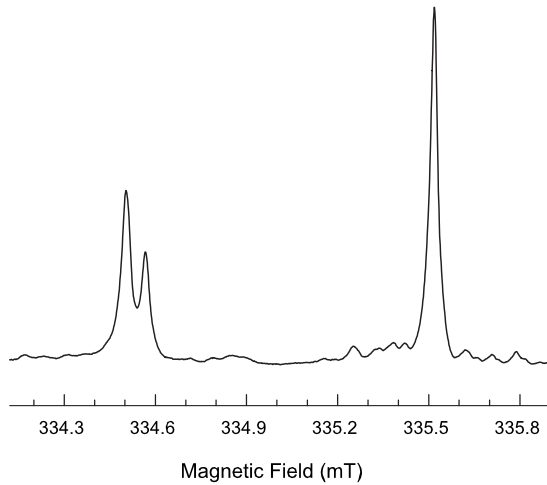


FIG. 1. EPR spectrum showing three photoinduced trapped hole centers in a fully oxidized TiO_2 (rutile) crystal. These data were taken at 4 K during exposure to 442 nm laser light. The magnetic field was along the [001] direction and the microwave frequency was 9.452 GHz.

As shown in Fig. 1, three holelike EPR signals are photoinduced at 4 K in our TiO_2 (rutile) samples. These data were taken while the 442 nm laser light was on the sample and the magnetic field was along the [001] crystal direction. For this orientation of field, the three EPR lines occur at 334.49, 334.57, and 335.51 mT and their linewidths are approximately 0.05 mT. All three signals are created by the light (i.e., they are not present before an illumination at low temperature when the sample is cooled in the dark). The three EPR lines in Fig. 1 do not have the usual first-derivative shape because the responsible $S=1/2$ spins have very long spin-lattice relaxation times and are easily saturated with microwave power. These trapped hole centers become thermally unstable at very low temperatures and thus are best observed with EPR near 4 K even though they are severely saturated at this temperature. Specifically, in our investigation, the trapped hole signals were always monitored at 4 K with the laser light on the sample and the phase-sensitive detector of the 100 kHz magnetic field modulation set out of phase.^{23–25} Concentrations of the photoinduced trapped holes are not estimated because of this nonconventional mode of spectrometer operation. Additional EPR signals due to singly ionized oxygen vacancies, neutral oxygen vacancies, Ti^{3+} - Si^{4+} centers, and Ti^{3+} self-trapped electrons also appear in our TiO_2 samples during illumination with 442 nm light at low temperature.² These electronlike spectra are easily saturated with microwave power at 4 K in single crystals. The three centers associated with oxygen vacancies and silicon are thermally more stable than the self-trapped electron center² and thus can be monitored at higher temperatures, between 20 and 30 K, where the effects of microwave power saturation are less pronounced. The Ti^{3+} self-trapped electron center is less stable and can only be observed at temperatures near and below 10 K.

The EPR signal at 335.51 mT in Fig. 1 is assigned to the self-trapped hole on the basis of its angular dependence. As shown in Fig. 2, data from this defect were acquired at 4 K in

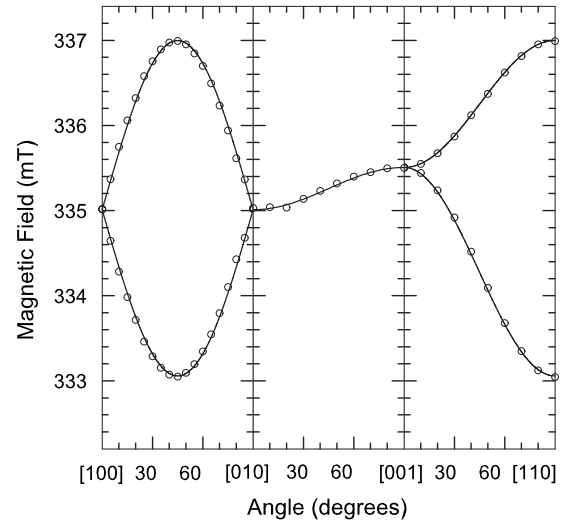


FIG. 2. Angular dependence of the EPR spectrum assigned to the self-trapped hole center in a fully oxidized TiO_2 crystal. These data were acquired in the three high-symmetry planes of the crystal. The measurement temperature was 4 K.

all three high-symmetry planes of the crystal. The sample was continuously illuminated with 442 nm light during the measurements. These plots provide information about the principal values and the principal-axis directions of the g matrix. The discrete points in Fig. 2 represent experimental results and the solid curves are computer generated using the final set of “best” parameters for the g matrix. Two important results are provided by the data in Fig. 2. First, only two crystallographically equivalent sites (i.e., orientations) for this defect are needed to explain the observed angular-dependence patterns. The two sites are magnetically equivalent when rotating from [010] to [001], and are magnetically inequivalent when rotating in the other two planes. This requires the principal axes of the g matrix to coincide with high-symmetry directions in the crystal. Second, the g shifts (deviations from the free-electron value of 2.0023) are positive and are relatively small. The following spin Hamiltonian, containing only the electron Zeeman term, was expressed as a 2×2 matrix and used in a least-squares fitting procedure to determine the best-fit parameters describing the data in Fig. 2,

$$\mathbf{H} = \beta \mathbf{S} \cdot \mathbf{g} \cdot \mathbf{B}. \quad (1)$$

The results of this fitting process are summarized in Table I where the principal values of the g matrix and the corresponding directions of the principal axes are given for one of the two crystallographically equivalent sites of the defect.

Our model for the self-trapped hole center in TiO_2 (rutile) is illustrated in Fig. 3. A photoinduced hole self-trapped in a nonbonding p orbital on an oxygen ion in the otherwise perfect lattice is consistent with the data in Fig. 2 and forms the basis of the model. A slight relaxation of the surrounding lattice provides the shallow potential well that localizes the hole on the one oxygen ion. In an earlier detailed computational study, Deskins and Dupuis¹⁰ predicted that this is the correct model for the intrinsic hole polaron in TiO_2 (rutile).

TABLE I. Spin-Hamiltonian parameters for the self-trapped hole center and one of the two extrinsic hole centers in a single crystal of TiO₂ (rutile). The principal axes listed below correspond to one of the two crystallographically equivalent sites for the self-trapped hole center and to one of the four crystallographically equivalent sites for the extrinsic hole center. The g_1 principal axis is perpendicular to the plane defined by the three cations immediately adjacent to the oxygen ion containing the hole (specified to be [110] for the sites described below). Directions of the principal axes for g_2 and g_3 are in the (110) plane (see the models in Figs. 3 and 5). The uncertainty in the directions of principal axes is $\pm 1^\circ$.

	Principal value	Principal-axis direction
Self-trapped hole center		
g_1	2.0040 ± 0.0001	[110]
g_2	2.0129 ± 0.0001	[001]
g_3	2.0277 ± 0.0001	[1 $\bar{1}$ 0]
Extrinsic (impurity-related) hole center		
g_1	2.0036 ± 0.0001	[110]
g_2	2.0182 ± 0.0001	14.5° from [001]
g_3	2.0307 ± 0.0001	14.5° from [1 $\bar{1}$ 0]

There are two equivalent distorted TiO₆ octahedra in the TiO₂ (rutile) lattice. These TiO₆ units are elongated in directions perpendicular to the [001] direction with the six oxygen ions separating into a set of two along the elongation direction and a set of four in the (110) planes perpendicular to the

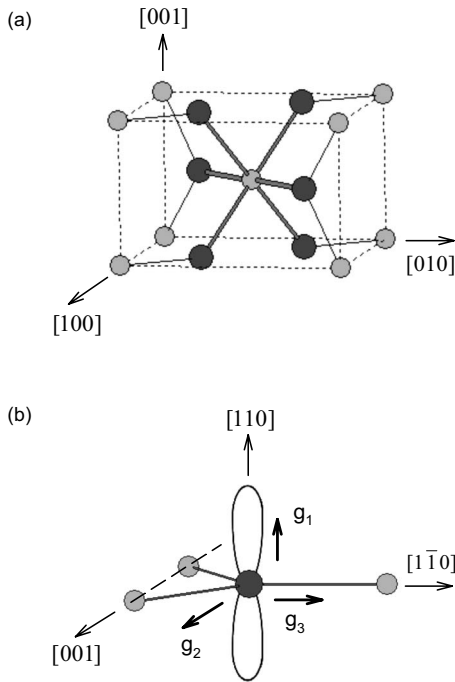


FIG. 3. Proposed model of the self-trapped hole center in a TiO₂ (rutile) crystal. (a) The regular rutile lattice. (b) The self-trapped hole localized in a nonbonding oxygen *p* orbital oriented perpendicular to the plane formed by the three nearest-neighbor titanium ions.

elongation direction. The two TiO₆ octahedra are related by a 90° rotation about the [001] direction. Figure 3(a) shows a portion of the rutile lattice containing one of these TiO₆ units. In our study, the focus is on the oxygen ions. All of the oxygen ions in TiO₂ (rutile) are crystallographically equivalent. As can be seen in Figs. 3(a) and 3(b), each oxygen ion has three neighboring titanium ions; two of these titanium neighbors are equivalent and are aligned along the [001] direction and the third titanium lies in one of the four $\langle 110 \rangle$ directions. The unpaired spin (i.e., the hole) in our paramagnetic center is localized in the nonbonding oxygen *p* orbital oriented perpendicular to the plane formed by the oxygen ion and the three titanium ions. This orientation allows the positive hole to avoid the three positively charged neighboring titanium ions and thus minimizes the ground-state energy of the defect. The local symmetry of the lattice requires that the *g* matrix associated with the unpaired spin in this nonbonding *p* orbital have principal axes along the [110], [001], and [1 $\bar{1}$ 0] directions [as shown for the site illustrated in Fig. 3(b)].

A simple analysis of the expected *g* matrix supports our model of a hole trapped in a nonbonding *p* orbital on an oxygen ion in the otherwise perfect lattice for the EPR signal at 335.51 mT in Fig. 1. Three discrete energy levels (E_1 , E_2 , and E_3 , in ascending order) are produced when the threefold orbital degeneracy of this 2P state ($L=1, S=1/2$) is removed by the crystalline electric field. The ordering in energy of these three levels is determined by the relative electrostatic repulsion effects on the *p* orbitals caused by the three neighboring Ti⁴⁺ ions. Referring to Fig. 3(b), E_1 has the lowest energy and corresponds to the *p* orbital aligned along the [110] direction, E_2 has the intermediate energy and corresponds to the *p* orbital aligned along the [001] direction, and E_3 has the highest energy and corresponds to the *p* orbital aligned along the [1 $\bar{1}$ 0] direction. Spin-orbit interactions mix the excited states with the ground state and give the following first-order expressions for the principal *g* values,²⁶

$$g_1 = g_e, \quad g_2 = g_e - \frac{2\lambda}{E_3 - E_1}, \quad g_3 = g_e - \frac{2\lambda}{E_2 - E_1}. \quad (2)$$

In Eq. (2), $g_e=2.0023$ and λ is the spin-orbit coupling constant (-135 cm^{-1} for an O⁻ ion). The energy differences E_2-E_1 and E_3-E_1 in the denominators correspond to possible optical-absorption bands associated with the trapped hole center. From Table I, we see that the experimental value of g_1 (2.0040) is very near to g_e (2.0023), as predicted by this first-order analysis. To partially account for covalency, an orbital reduction factor k is often introduced that reduces the spin-orbit constant ($\lambda'=k\lambda$). We take k to be 0.6, thus making $\lambda'=-81 \text{ cm}^{-1}$. Substituting the measured g_2 and g_3 values from Table I into Eq. (2) and replacing λ with λ' gives $E_2-E_1=6380 \text{ cm}^{-1}$ ($\sim 1570 \text{ nm}$) and $E_3-E_1=15300 \text{ cm}^{-1}$ ($\sim 654 \text{ nm}$). These energy differences suggest that the self-trapped hole center may have weak (i.e., low oscillator strength) optical-absorption bands in the near infrared and visible portions of the spectrum.

We recently suggested a model for the self-trapped hole center in TiO₂ (rutile) that had the hole shared by two oxy-

gen ions.² We now consider this to be a less likely possibility and prefer a single oxygen trapping site for the hole.^{10–12} As can be seen in Fig. 3(a), there are two pairs of oxygen ions that might share the hole; one pair has a small separation and is aligned along the $\langle 110 \rangle$ directions while the other pair has a larger separation and is aligned along the $[001]$ direction. For each pair, the trapped hole's energy is lowered when the two oxygen ions sharing the hole move together (i.e., forming a shallow potential well due to lattice relaxation). This decrease in energy caused by relaxation is, however, offset by the increased electrostatic repulsion energy between the hole and the adjacent Ti^{4+} ions. A trapped hole shared by two anions is a common defect in alkali halide crystals but is not often observed in oxide crystals.

A set of less intense EPR lines extending out approximately 0.3 mT on either side of the self-trapped hole signal at 335.51 mT in Fig. 1 are tentatively assigned to weak hyperfine interactions with nearest-neighbor ^{47}Ti and ^{49}Ti nuclei (^{47}Ti is 7.4% abundant with $I=5/2$ and ^{49}Ti is 5.4% abundant with $I=7/2$). Unfortunately, these hyperfine lines in Fig. 1 are not well resolved and it is difficult to determine whether one, two, or three neighboring titanium ions are contributing to the spectrum. Also, the pattern is not symmetrical about the center line, which suggests that some of the observed lines may be “forbidden” transitions ($\Delta m_S = \pm 1$ and $\Delta m_I = \pm 1$ or ± 2). Forbidden transitions are often seen when the hyperfine and the nuclear electric quadrupole terms in a spin Hamiltonian have similar magnitudes.

The two EPR signals at lower field (334.49 and 334.57 mT) in Fig. 1 are assigned to trapped hole centers that have adjacent unidentified defects. Direct evidence that these trapped holes occupy sites with a local symmetry lower than the perfect lattice comes from their EPR angular-dependence patterns. Because the two centers exhibit similar patterns, we studied only the more intense signal at 334.49 mT in detail. Data from this extrinsic hole center were acquired at 4 K in all three high-symmetry planes of the crystal, as shown in Fig. 4. The sample was continuously illuminated with 442 nm light during the measurements. The discrete points in Fig. 4 represent experimental results and the solid curves are computer generated using the final set of “best” parameters for the g matrix. In contrast to the self-trapped hole center described earlier in this paper, four crystallographically equivalent sites are required to explain the g matrix angular-dependence data in Fig. 4 for the extrinsic trapped hole center. These four sites are pairwise magnetically equivalent when rotating the magnetic field from $[100]$ to $[010]$ and from $[010]$ to $[001]$. The four sites divide into three sets when rotating from $[001]$ to $[110]$. The simplest explanation for these four crystallographically equivalent sites is a defect complex consisting of a hole on an oxygen ion and an impurity ion replacing one of the two equivalent neighboring titanium ions aligned along the $[001]$ axis. Our proposed model, illustrated in Fig. 5, follows directly from the earlier studies of trapped hole centers in GeO_2 doped with aluminum¹³ and TiO_2 doped with aluminum or gallium.^{14,15} The spin Hamiltonian in Eq. (1) and the angular-dependence data in Fig. 4 were used in a least-squares fitting procedure to determine the principal values and principal-axis directions for this extrinsic (impurity-related) hole center. These results are summarized in Table I.

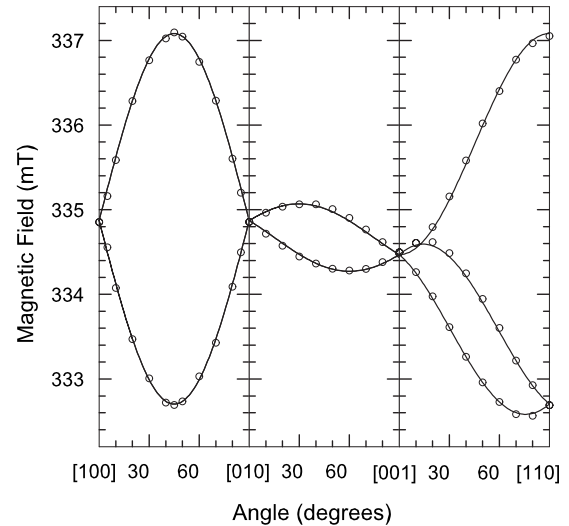


FIG. 4. Angular dependence of the EPR spectrum assigned to an extrinsic (impurity-related) hole center in TiO_2 . These data were acquired at 4 K in the three high-symmetry planes of the crystal.

The identity of the adjacent defect for this lower-symmetry trapped hole center is not established in our study. In Fig. 5, it is designated as an X^{3+} cation replacing a Ti^{4+} ion. There are no resolved hyperfine lines in the EPR spectrum, which strongly argues against Al^{3+} , Ga^{3+} , In^{3+} , and Sc^{3+} impurity ions. One possibility is an Y^{3+} ion. It is only slightly larger than a Ti^{4+} ion and is a moderately abundant element in nature. Although yttrium has a magnetic nucleus ($I=1/2$, 100% abundant), its nuclear magnetic moment is relatively small and the expected hyperfine doublet splitting would be comparable to the observed linewidth for our extrinsic trapped hole center and thus unresolved. In a similar example, a trapped hole on an oxygen ion next to two Y^{3+} ions in a YVO_4 crystal gave no resolved hyperfine with the ^{89}Y nuclei.²⁷ It is also possible that a tetravalent impurity ion

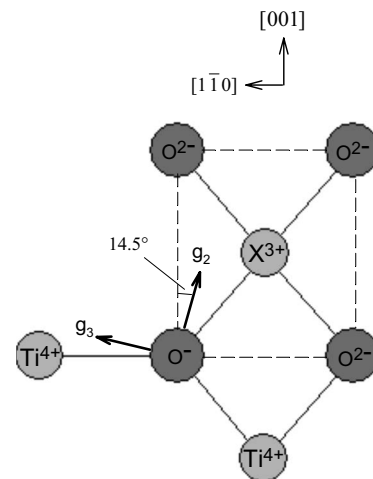


FIG. 5. Proposed model of the extrinsic (impurity-related) hole center in a TiO_2 (rutile) crystal. A projection on the (110) plane is shown. The unpaired spin in the nonbonding oxygen p orbital at the O^- site is aligned along the $[110]$ direction (i.e., perpendicular to the plane of the figure).

such as Zr^{4+} or Si^{4+} or a divalent impurity ion such as Mg^{2+} could be the defect adjacent to this extrinsic trapped hole center in TiO_2 (rutile).

A final point to be addressed is the thermal stability of the photoinduced trapped hole centers in TiO_2 (rutile). At 4 K, the three EPR hole signals reported in this paper thermally decay at approximately the same rate when the laser light is removed. They do not, however, completely disappear. Instead, they reach new reduced equilibrium concentrations and remain at these new lower concentrations for tens of minutes or longer. The portion of each center disappearing within a few seconds at 4 K varies from 85% to 50%, depending on the time the laser light was on prior to its removal. A larger percentage decays quickly when the laser light is on for a shorter period of time. The remaining portions of the three hole signals (those that are semistable at 4 K) disappear in the dark within 1 or 2 min when the temperature is raised to approximately 10 K. These results suggest that the activation energies for the photoinduced hole centers may be in the 10–20 meV range. Ordinarily, the equilibrium photoinduced concentrations of these hole centers will depend on both the incident laser power (the production rate) and the sample temperature (the decay rate). It appears in the present study that the separation distance between a trapped hole center and a charge-compensating trapped electron center is also an important parameter in determining the rate at which the hole centers decay. We suggest that the majority of trapped electrons during an illumination at 4 K form self-trapped electron centers. As the illumination time at 4 K increases, the average separation distance between the

trapped hole centers and the self-trapped electron centers is expected to increase. This results in a reduced recombination rate at 4 K and explains the smaller percentage of hole centers that decay at 4 K when the laser light is removed after a longer illumination time. In general, it appears that isolated (i.e., well separated) self-trapped holes and self-trapped electrons produced by laser light in TiO_2 (rutile) independently become unstable near 10 K in the dark as they thermally release their trapped charge.^{1,2} Significant decays of these defects in the dark at temperatures below 10 K are most likely related to the close proximity of the trapped holes and electrons.

In summary, EPR spectra from trapped hole centers are produced in TiO_2 (rutile) crystals during illumination at 4 K with 442 nm laser light. One spectrum has the symmetry of the rutile lattice and is assigned to a self-trapped hole center while two other spectra have a lower local symmetry and are assigned to extrinsic (defect-related) trapped hole centers. In each case, the hole is localized on one oxygen ion. The corresponding electron traps are primarily self-trapped electron centers. These photoinduced trapped holes and self-trapped electrons become thermally unstable at very low temperature and their decay rates depend on illumination times and temperature. Even at room temperature, illumination with near-band-edge light will produce these fundamental hole and electron centers but they will rapidly recombine or migrate to more stable trapping sites.

This research was supported by Grant No. DMR-0804352 from the National Science Foundation.

*Corresponding author; larry.halliburton@mail.wvu.edu

¹S. Yang and L. E. Halliburton, *Phys. Rev. B* **81**, 035204 (2010).

²S. Yang, L. E. Halliburton, A. Manivannan, P. H. Bunton, D. B. Baker, M. Klemm, S. Horn, and A. Fujishima, *Appl. Phys. Lett.* **94**, 162114 (2009).

³F. D. Brandão, M. V. B. Pinheiro, G. M. Ribeiro, G. Medeiros-Ribeiro, and K. Krambrock, *Phys. Rev. B* **80**, 235204 (2009).

⁴M. Aono and R. R. Hasiguti, *Phys. Rev. B* **48**, 12406 (1993).

⁵J. Kerssen and J. Volger, *Physica (Amsterdam)* **69**, 535 (1973).

⁶P. F. Chester, *J. Appl. Phys.* **32**, 2233 (1961).

⁷H. J. Gerritsen, S. E. Harrison, H. R. Lewis, and J. P. Wittke, *Phys. Rev. Lett.* **2**, 153 (1959).

⁸D. L. Carter and A. Okaya, *Phys. Rev.* **118**, 1485 (1960).

⁹G. J. Lichtenberger and J. R. Addison, *Phys. Rev.* **184**, 381 (1969).

¹⁰N. A. Deskins and M. Dupuis, *J. Phys. Chem. C* **113**, 346 (2009).

¹¹D. Muñoz Ramo, A. L. Shluger, J. L. Gavartin, and G. Bersuker, *Phys. Rev. Lett.* **99**, 155504 (2007).

¹²O. F. Schirmer, *J. Phys.: Condens. Matter* **18**, R667 (2006).

¹³M. Stapelbroek, R. H. Bartram, O. R. Gilliam, and D. P. Madacs, *Phys. Rev. B* **13**, 1960 (1976).

¹⁴D. Zwingel, *Solid State Commun.* **20**, 397 (1976).

¹⁵D. Zwingel, *Solid State Commun.* **26**, 775 (1978).

¹⁶A. Stashans and S. Bermeo, *Chem. Phys.* **363**, 100 (2009).

¹⁷B. J. Morgan and G. W. Watson, *Phys. Rev. B* **80**, 233102 (2009).

¹⁸A. Fujishima, X. Zhang, and D. A. Tryk, *Surf. Sci. Rep.* **63**, 515 (2008).

¹⁹J. Tang, J. R. Durrant, and D. R. Klug, *J. Am. Chem. Soc.* **130**, 13885 (2008).

²⁰Y. Tamaki, A. Furube, M. Murai, K. Hara, R. Katoh, and M. Tachiya, *Phys. Chem. Chem. Phys.* **9**, 1453 (2007).

²¹S. Livraghi, M. C. Paganini, E. Giamello, A. Selloni, C. Di Valentini, and G. Pacchioni, *J. Am. Chem. Soc.* **128**, 15666 (2006).

²²T. Berger, M. Sterrer, O. Diwald, E. Knozinger, D. Panayotov, T. L. Thompson, and J. T. Yates, *J. Phys. Chem. B* **109**, 6061 (2005).

²³J. R. Harbridge, G. A. Rinard, R. W. Quine, S. S. Eaton, and G. R. Eaton, *J. Magn. Reson.* **156**, 41 (2002).

²⁴Y. Jiang, N. C. Giles, and L. E. Halliburton, *J. Appl. Phys.* **101**, 093706 (2007).

²⁵S. M. Evans, N. C. Giles, L. E. Halliburton, and L. A. Kappers, *J. Appl. Phys.* **103**, 043710 (2008).

²⁶J. E. Wertz and J. R. Bolton, *Electron Spin Resonance: Elementary Theory and Practical Applications* (McGraw-Hill, New York, 1972), pp. 278–281.

²⁷N. Y. Garces, L. E. Halliburton, K. T. Stevens, M. Shone, and G. K. Foundos, *J. Appl. Phys.* **91**, 1354 (2002).